

# Frame element with lateral deformable supports: Formulations and numerical validation

Suchart Limkatanyu <sup>a,\*</sup>, Enrico Spacone <sup>b,1</sup>

<sup>a</sup> Department of Civil Engineering, Faculty of Engineering, Prince of Songkla University, Songkhla 90110, Thailand

<sup>b</sup> Department of PRICOS, Faculty of Architecture, University "G. D'Annunzio", 65127 Pescara, Italy

Received 5 November 2004; accepted 6 December 2005

Available online 20 March 2006

## Abstract

This paper presents the theory and the numerical validation of three different formulations of nonlinear frame elements with nonlinear lateral deformable supports. The governing differential equations of the problem are derived first and the three different finite element formulations are then presented. The first model follows a displacement-based formulation, which is based on the virtual displacement principle. The second one follows the force-based formulation, which is based on the virtual force principle. The third model follows the Hellinger–Reissner mixed formulation, which is based on the two-field mixed variational principle. The selection of the displacement and force interpolation functions for the different formulations is discussed. Tonti's diagrams are used to conveniently represent the equations governing both the strong and the weak forms of the problem. The general matrix equations of the three formulations are presented, with some details on the issues regarding the elements' implementations in a general-purpose finite element program. The convergence, accuracy, and computational times of the three elements are studied through a numerical example. The distinctive element characteristics in terms of force and deformation discontinuities between adjacent elements are discussed. The capability of the proposed frame models to trace the softening response due to softening of the foundation is also investigated. Overall, the force-based and the mixed models are much more accurate than the displacement-based model and require very few elements to reach the converged solution. The force-based element is slightly more accurate than the mixed model, but it is more prone to numerical instabilities as it involves inverting the element flexibility matrix.

© 2006 Elsevier Ltd. All rights reserved.

**Keywords:** Beam elements; Soil–pile interaction; Beam on Winkler foundation; Displacement-based formulation; Force-based formulation; Mixed formulation

## 1. Introduction

When structures undergo seismic excitations, the intensity of the forces applied to the structural system (framework and pile foundation) depends on both the stiffness of the framework (superstructure) and the lateral stiffness of the pile foundation. The accurate modeling of the soil–pile system is thus important in predicting the response

of new structural systems under both static and dynamic loadings as well as in assessing the residual stiffness and strength of existing structural systems after a severe earthquake. Even for very simple systems, considering the soil–pile system leads to a more realistic estimation of the fundamental period of the structural system.

Unlike frame (superstructure) design and analysis, where members can be considered as separate elements connected at the joints, in the pile–foundation design the pile must be considered in conjunction with the surrounding soil. As the piles try to displace inside the surrounding soil, the latter needs to displace and thus provides a resisting force. The force interaction between the pile and the

\* Corresponding author. Tel.: +66 74 287129; fax: +66 74 212891.

E-mail addresses: [lsuchart@ratree.psu.ac.th](mailto:lsuchart@ratree.psu.ac.th) (S. Limkatanyu), [e.spacone@unich.it](mailto:e.spacone@unich.it) (E. Spacone).

<sup>1</sup> Tel.: +39 085 4537276; fax: +39 085 4537255.

surrounding soil results in a change of the internal forces in the pile. Consequently, the inclusion of the soil–pile system into the numerical model is an important step toward the development of accurate nonlinear techniques for design and analysis of the structural systems under both static and dynamic loadings.

Several analytical models have been proposed in the published literature to study the problem of the soil–structure interaction. These models range from comparatively simple approaches in which the surrounding soils are represented as a set of discrete springs, to sophisticated three-dimensional finite element models. These analytical models are classified here into three categories: (a) elastic continuum models; (b) solid (2-D or 3-D) finite element models; (c) line (1-D) frame elements based on the beam theory. The *elastic continuum model* was first proposed by Mindlin [1] to study the problem of a beam on an elastic foundation representing the soil. Because of the similarity between the beam problem and the pile problem, the Mindlin’s solution is adopted by several researchers (e.g. [2,3]) to study the problem of laterally loaded piles. The elastic continuum model, however, is limited by several factors. Its main drawback is due to the assumption that the surrounding soil is elastic. At small deflections, a linear soil behavior is acceptable. Nevertheless, the behavior of the surrounding soil is highly nonlinear under moderate and large deflections. Several examples and applications of *solid finite elements* developed for analysis of laterally loaded piles are found in Desai and Appel [4], Kuhlemeyer [5], Winnicki and Zienkiewicz [6] and more recently, Yang and Jeremic [7]. Analyses performed with solid elements provide greater details but are hampered by higher computational costs. Only foundation components or small structural systems can be realistically investigated using solid finite element models. For the nonlinear analysis of large structural systems under monotonic and cyclic loadings, *line frame elements* represent a good compromise between accuracy and computational speed. Consequently, this work focuses on the development of a new family of 1-D frame elements for pile members with lateral soil.

The pile element proposed by Budek et al. [8] consists of a Hermitian beam element representing the pile, plus element-end springs representing the surrounding soils. Due to the discrete nature of the soil springs, a large number of elements are needed to gain sufficient accuracy. Hoit et al. [9] modified the discrete-element model proposed by Mitchell [10] by attaching nonlinear soil springs at the element ends to study the problem of pile–soil interactions. The discrete-element model is made up of four main components. There are two blocks in the middle, which can extend and twist with respect to each other. Each of these middle blocks is linked by springs to a rigid end block. These spring connections represent the axial, torsion and bending actions. Though simple, this model requires the formations of ad hoc phenomenological force–deformation laws for the spring connections.

The main objective of this paper is to propose a set of line elements with distributed soil–structure interaction. The elements are based on different formulations stemming from those developed by Limkatanyu and Spacone [11] to model bond-slip effects in reinforced concrete frame elements. The derivation of the governing differential equations of the frame element with lateral deformable supports is presented first. Next, three different element formulations are presented: displacement-based, force-based and two-field mixed formulation. The implementation issues of the three different formulations in a general-purpose nonlinear structural analysis program are discussed in Limkatanyu and Spacone [12]. The frame elements with lateral deformable supports presented in this work are different from those published to date in that the lateral soil is represented by continuous springs along the element length. The soil pressure at any point is directly related to the lateral displacement at that point, thus following the Winkler foundation concept. The elements proposed in this work are implemented in the general-purpose finite element code FEAP [13].

## 2. Equations of frame element with lateral deformable supports (strong form)

### 2.1. Equilibrium

The free body diagram of an infinitesimal segment  $dx$  of frame element with lateral deformable supports (e.g. soil) is shown in Fig. 1. Only soil stresses normal to the beam are taken into account in this study. Based on the small-deformation assumption, all of the equilibrium conditions are considered in the undeformed configuration. Axial equilibrium in the beam component leads to the following equation:

$$\frac{dN(x)}{dx} = 0 \tag{1}$$

where  $N(x)$  is the axial force in the beam. Vertical equilibrium of the infinitesimal segment  $dx$  yields

$$\frac{dV(x)}{dx} - p_y(x) + D_s^{top}(x) + D_s^{bottom}(x) = 0 \tag{2}$$

where  $V(x)$  is the beam-section shear force;  $p_y(x)$  is the transverse distributed load;  $D_s^{top}(x)$  and  $D_s^{bottom}(x)$  are the

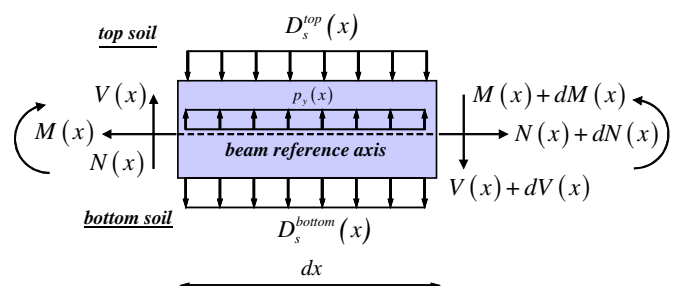


Fig. 1. Beam element with lateral deformable supports.

lateral soil-forces at the top and bottom faces of the beam, respectively. Finally, moment equilibrium yields

$$\frac{dM(x)}{dx} - V(x) = 0 \quad (3)$$

where  $M(x)$  is the beam-section bending moment. This work follows the Euler–Bernoulli beam theory, thus the shear deformations are neglected. The shear force  $V(x)$  is removed by combining Eqs. (2) and (3) to obtain

$$\frac{d^2M(x)}{dx^2} - p_y(x) + D_s^{\text{top}}(x) + D_s^{\text{bottom}}(x) = 0 \quad (4)$$

Eqs. (1) and (4) represent the governing equilibrium equations of the frame element with lateral deformable supports. Eqs. (1) and (4) can be expressed in the following matrix form:

$$\hat{\partial}_B^T \mathbf{D}_B(x) + \hat{\partial}_s^T \mathbf{D}_s(x) - \mathbf{p}(x) = \mathbf{0} \quad (5)$$

where  $\mathbf{D}_B(x) = \{N(x) \quad \vdots \quad M(x)\}^T$  are the element section forces,  $\mathbf{D}_s(x) = \{D_s^{\text{top}}(x) \quad \vdots \quad D_s^{\text{bottom}}(x)\}^T$  are the soil-forces at section  $x$  and  $\mathbf{p}(x) = \{0 \quad \vdots \quad p_y(x)\}^T$  is the element force vector.  $\hat{\partial}_B$  and  $\hat{\partial}_s$  are beam and soil differential operators, respectively and are defined as

$$\hat{\partial}_B = \begin{bmatrix} \frac{d}{dx} & 0 \\ 0 & \frac{d^2}{dx^2} \end{bmatrix}; \quad \hat{\partial}_s = \begin{bmatrix} 0 & 1 \\ 0 & 1 \end{bmatrix} \quad (6)$$

It is interesting to observe that there are four internal force unknowns while only two equilibrium equations are available at any element section. Consequently, this system is internally statically indeterminate and the internal forces cannot be determined simply by the equilibrium conditions.

## 2.2. Compatibility

The element section deformation vector conjugate of  $\mathbf{D}_B(x)$  is  $\mathbf{d}_B(x) = \{\varepsilon_B(x) \quad \vdots \quad \kappa_B(x)\}^T$ , where  $\varepsilon_B(x)$  is the beam-section axial strain at the reference axis and  $\kappa_B(x)$  is the beam-section bending curvature. The displacement vector  $\mathbf{u}(x) = \{u_B(x) \quad v_B(x)\}^T$  contains the displacement fields along the element, that is  $u_B(x)$  and  $v_B(x)$ , the beam axial and transverse displacements, respectively.

From the small-deformation assumption, the element deformations are related to the element displacements through the following compatibility relations:  $\varepsilon_B(x) = du_B(x)/dx$  and  $\kappa_B(x) = d^2v_B(x)/dx^2$ , which can be expressed in the following matrix form:

$$\mathbf{d}_B(x) = \hat{\partial}_B \mathbf{u}(x) \quad (7)$$

Based on the Winkler foundation theory, which assumes perfect compatibility between beam and soil displacements, the lateral-soil deformations are determined through the following compatibility relations:

$$\begin{aligned} d_s^{\text{top}}(x) &= v_B(x) \\ d_s^{\text{bottom}}(x) &= v_B(x) \end{aligned} \quad (8)$$

where  $d_s^{\text{top}}(x)$  and  $d_s^{\text{bottom}}(x)$  are the lateral-soil deformations at the top and bottom faces, respectively. If the soil deformation vector  $\mathbf{d}_s(x) = \{d_s^{\text{top}}(x) \quad \vdots \quad d_s^{\text{bottom}}(x)\}^T$  is defined, Eq. (8) can be expressed in the following matrix form:

$$\mathbf{d}_s(x) = \hat{\partial}_s \mathbf{u}(x) \quad (9)$$

## 2.3. Force–deformation relations

The nonlinear nature of the proposed elements derives entirely from the nonlinear relation between the section forces  $\mathbf{D}_B(x)$ ,  $\mathbf{D}_s(x)$  and the section deformation  $\mathbf{d}_B(x)$ ,  $\mathbf{d}_s(x)$ . In the proposed formulations, the fiber section model is used to derive the beam-section constitutive law  $\mathbf{D}_B = \mathbf{D}_B(\mathbf{d}_B)$ . The fiber model automatically accounts for the interaction between axial and bending responses and can be used to model reinforced concrete, steel and other kinds of composite piles. The explicit expression for the fiber beam-section force–deformation relation is given in Spacone et al. [14]. For the lateral-soil constitutive relations  $\mathbf{D}_s = \mathbf{D}_s(\mathbf{d}_s)$ , a generic spring model is used here. Further details will be given in the numerical examples. The section and lateral-soil nonlinear laws are linearized according to the following forms:

$$\mathbf{D}_B(x) = \mathbf{D}_B^0(x) + \Delta \mathbf{D}_B(x) = \mathbf{D}_B^0(x) + \mathbf{k}_B^0(x) \Delta \mathbf{d}_B(x) \quad (10)$$

$$\mathbf{D}_s(x) = \mathbf{D}_s^0(x) + \Delta \mathbf{D}_s(x) = \mathbf{D}_s^0(x) + \mathbf{k}_s^0(x) \Delta \mathbf{d}_s(x)$$

where  $\mathbf{k}_B(x)$ ,  $\mathbf{k}_s(x)$  are the section and soil stiffness matrices, respectively. The consistent inverse of (10) can be expressed in the following form:

$$\mathbf{d}_B(x) = \mathbf{d}_B^0(x) + \Delta \mathbf{d}_B(x) = \mathbf{d}_B^0(x) + \mathbf{f}_B^0(x) \Delta \mathbf{D}_B(x) \quad (11)$$

$$\mathbf{d}_s(x) = \mathbf{d}_s^0(x) + \Delta \mathbf{d}_s(x) = \mathbf{d}_s^0(x) + \mathbf{f}_s^0(x) \Delta \mathbf{D}_s(x)$$

where  $\mathbf{f}_B(x)$ ,  $\mathbf{f}_s(x)$  are the section and soil flexibility matrices, respectively. In the above equations and for the rest of the paper, superscript 0 indicates the value of a vector or matrix at the initial point of a linearized nonlinear scheme.

The compatibility, equilibrium and constitutive equations for the frame element with distributed lateral deformable supports presented above are conveniently represented in the classical Tonti's diagram of Fig. 2. This diagram is going to be modified for the weak forms obtained with different element formulations. Finally, for the sake of brevity, the transverse load  $p_y(x)$  is omitted in the following derivations.

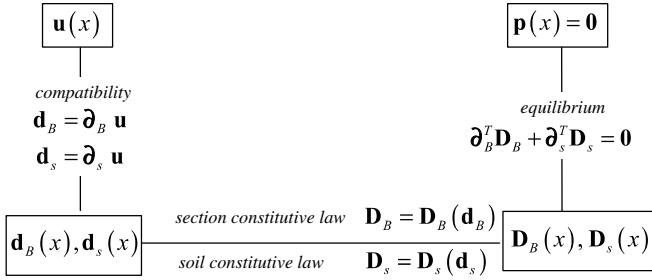


Fig. 2. Tonti's diagram for beam with lateral deformable supports: governing differential equations (strong form).

### 3. Finite element formulations (weak form)

Three different finite element formulations are presented in this paper: (a) a displacement-based formulation; (b) a hybrid force-based formulation; (c) a two-field mixed formulation.

#### 3.1. Displacement-based formulation

The displacement-based formulation is summarized in the Tonti's diagram of Fig. 3. The element nodal displacements  $\mathbf{U}$  serve as the primary element variables. The section displacements  $\mathbf{u}(x)$  are related to the element nodal displacements through appropriate displacement interpolation functions. The section deformations  $\mathbf{d}_B(x)$  and soil-deformations  $\mathbf{d}_s(x)$  are determined through the beam compatibility (7) and the soil-interface compatibility (9), respectively. Therefore, the compatibility conditions are imposed point-wise. On the other hand, the equilibrium equations (5) are only expressed in the weighted integral form through the virtual displacement principle as

$$\int_L \delta \mathbf{u}^T(x) (\partial_B^T \mathbf{D}_B(x) + \partial_s^T \mathbf{D}_s(x)) dx = 0 \quad (12)$$

where  $\delta \mathbf{u}(x)$  represents a virtual displacement field. Upon substitution of the section linearized constitutive laws (10), Eq. (12) is written

$$\int_L \delta \mathbf{u}^T(x) \{ \partial_B^T (\mathbf{D}_B^0(x) + \mathbf{k}_B^0(x) \partial_B \Delta \mathbf{u}(x)) + \partial_s^T (\mathbf{D}_s^0(x) + \mathbf{k}_s^0(x) \partial_s \Delta \mathbf{u}(x)) \} dx = 0 \quad (13)$$

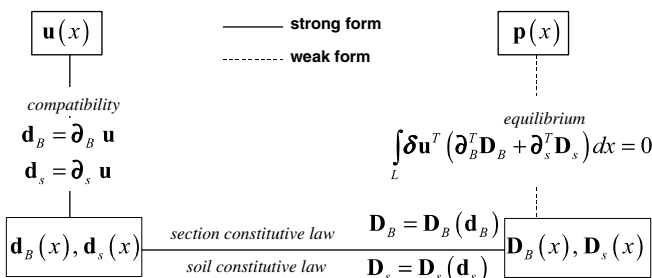


Fig. 3. Tonti's diagram for beam with lateral deformable supports: displacement-based formulation.

In order to move the differential operators  $\partial_B$  and  $\partial_s$  from the force vectors  $\mathbf{D}_B(x)$  and  $\mathbf{D}_s(x)$  to the virtual displacement fields  $\delta \mathbf{u}(x)$ , integration by parts is applied to Eq. (13), resulting in

$$\int_L \left\{ \begin{matrix} \partial_B(\delta \mathbf{u}(x)) \\ \partial_s(\delta \mathbf{u}(x)) \end{matrix} \right\}^T \begin{bmatrix} \mathbf{k}_B^0(x) & \mathbf{0} \\ \mathbf{0} & \mathbf{k}_s^0(x) \end{bmatrix} \left\{ \begin{matrix} \partial_B(\Delta \mathbf{u}(x)) \\ \partial_s(\Delta \mathbf{u}(x)) \end{matrix} \right\} dx = \delta \mathbf{U}^T \mathbf{P} - \int_L (\partial_B(\delta \mathbf{u}^T(x)) \mathbf{D}_B^0(x) + \partial_s(\delta \mathbf{u}^T(x)) \mathbf{D}_s^0(x)) dx \quad (14)$$

where  $\delta \mathbf{U}^T \mathbf{P}$  derives from the boundary terms and represents the external virtual work done by the virtual nodal displacements  $\delta \mathbf{U}$  on the externally applied nodal forces  $\mathbf{P}$ . Eq. (14) is the fundamental equation for the displacement-based finite element formulation of the frame element with lateral deformable supports. The element displacements  $\mathbf{u}(x)$  are related to the nodal displacements  $\mathbf{U}$  through the displacement interpolation functions  $\mathbf{N}_u^{\text{D-B}}(x)$

$$\mathbf{u}(x) = \mathbf{N}_u^{\text{D-B}}(x) \mathbf{U} \quad (15)$$

where the superscript D-B denotes the displacement-based formulation. It follows that  $\mathbf{d}_B(x) = \mathbf{B}_B^{\text{D-B}}(x) \mathbf{U}$  and  $\mathbf{d}_s(x) = \mathbf{B}_s^{\text{D-B}}(x) \mathbf{U}$ , where  $\mathbf{B}_B^{\text{D-B}}(x) = \partial_B \mathbf{N}_u^{\text{D-B}}(x)$  and  $\mathbf{B}_s^{\text{D-B}}(x) = \partial_s \mathbf{N}_u^{\text{D-B}}(x)$ . Upon substitution of (15) into (14) and from the arbitrariness of  $\delta \mathbf{U}$

$$\int_L \left\{ \begin{matrix} \mathbf{B}_B^{\text{D-B}}(x) \\ \mathbf{B}_s^{\text{D-B}}(x) \end{matrix} \right\}^T \begin{bmatrix} \mathbf{k}_B^0(x) & \mathbf{0} \\ \mathbf{0} & \mathbf{k}_s^0(x) \end{bmatrix} \left\{ \begin{matrix} \mathbf{B}_B^{\text{D-B}}(x) \\ \mathbf{B}_s^{\text{D-B}}(x) \end{matrix} \right\} dx \Delta \mathbf{U} = \mathbf{P} - \int_L \mathbf{B}_B^{\text{D-B}^T}(x) \mathbf{D}_B^0(x) dx - \int_L \mathbf{B}_s^{\text{D-B}^T}(x) \mathbf{D}_s^0(x) dx \quad (16)$$

Eq. (16) is written in the compact form

$$\mathbf{K}^0 \Delta \mathbf{U} = \mathbf{P} - \mathbf{Q}^0 \quad (17)$$

$\mathbf{K}^0$  is the element stiffness matrix

$$\mathbf{K}^0 = \mathbf{K}_B^0 + \mathbf{K}_s^0 \quad (18)$$

where  $\mathbf{K}_B^0$  and  $\mathbf{K}_s^0$  are the beam and soil contributions, respectively, to the element stiffness matrix

$$\mathbf{K}_B^0 = \int_L \mathbf{B}_B^{\text{D-B}^T}(x) \mathbf{k}_B^0(x) \mathbf{B}_B^{\text{D-B}}(x) dx \quad (19)$$

$$\mathbf{K}_s^0 = \int_L \mathbf{B}_s^{\text{D-B}^T}(x) \mathbf{k}_s^0(x) \mathbf{B}_s^{\text{D-B}}(x) dx$$

$\mathbf{Q}^0$  contains the element resisting forces

$$\mathbf{Q}^0 = \mathbf{Q}_B^0 + \mathbf{Q}_s^0 \quad (20)$$

where  $\mathbf{Q}_B^0$  and  $\mathbf{Q}_s^0$  are the beam and soil contributions, respectively, to the element resisting forces

$$\mathbf{Q}_B^0 = \int_L \mathbf{B}_B^{\text{D-B}^T}(x) \mathbf{D}_B^0(x) dx \quad (21)$$

$$\mathbf{Q}_s^0 = \int_L \mathbf{B}_s^{\text{D-B}^T}(x) \mathbf{D}_s^0(x) dx$$

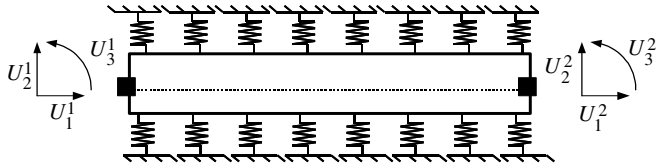


Fig. 4. Two-node displacement-based frame element with lateral deformable supports.

The right-hand side of (17) is the force residual corresponding to the weak statement of the equilibrium equation (5) and vanishes when the equilibrium configuration is reached.

The element used in this paper comprises a two-node beam with top and bottom soil interfaces (Fig. 4). The two-node element has a linear axial displacement field, a cubic transverse displacement field, and cubic soil-deformation fields along the interfaces. These proposed displacement fields satisfy the  $C^0$  and  $C^1$  continuities for the axial and transverse displacements required by the variational indices in (13). The two-node displacement-based element, though numerically stable, is not very accurate and is used primarily as reference model for the following, more advanced formulations.

### 3.2. Force-based (force-hybrid) formulation

The force-based formulation stems from the force-based steel–concrete composite beam element with partial interaction proposed by Salari et al. [15]. The force-based formulation is derived from the virtual force principle and is the dual of the displacement-based formulation. The steps involved in the force-based formulation are schematically represented in the Tonti ‘s diagram of Fig. 5. The element internal force fields  $\mathbf{D}_B(x)$  and  $\mathbf{D}_s(x)$  serve as the primary variables and are expressed in terms of the element nodal forces through appropriate force interpolation functions. The force interpolation functions are derived such that the equilibrium equations (5) are satisfied point-wise along the element. On the other hand, the beam compatibility equation (7) and the soil compatibility equation (9) are expressed only in the weighted integral form

$$\int_L \delta \mathbf{D}_B^T(x) (\mathbf{d}_B(x) - \partial_B \mathbf{u}(x)) dx + \int_L \delta \mathbf{D}_s^T(x) (\mathbf{d}_s(x) - \partial_s \mathbf{u}(x)) dx = 0 \quad (22)$$

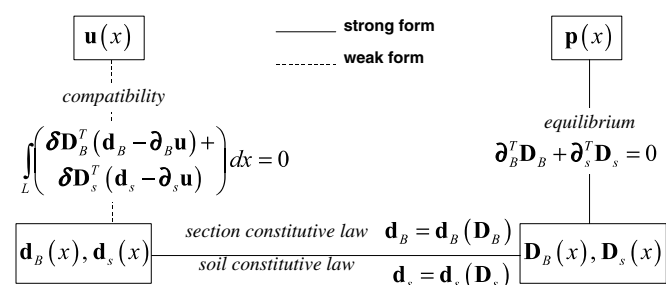


Fig. 5. Tonti’s diagram for beam with lateral deformable supports: force-based formulation.

where  $\delta \mathbf{D}_B(x)$  and  $\delta \mathbf{D}_s(x)$  are virtual equilibrated section and soil-interface force fields, respectively,. Upon substitution of the section linearized laws (11), Eq. (22) is written

$$\int_L \delta \mathbf{D}_B^T(x) (\mathbf{d}_B^0(x) + \mathbf{f}_B^0(x) \Delta \mathbf{D}_B(x) - \partial_B \mathbf{u}(x)) dx + \int_L \delta \mathbf{D}_s^T(x) (\mathbf{d}_s^0(x) + \mathbf{f}_s^0(x) \Delta \mathbf{D}_s(x) - \partial_s \mathbf{u}(x)) dx = 0 \quad (23)$$

where  $\mathbf{f}_B^0(x)$  and  $\mathbf{f}_s^0(x)$  are the initial flexibility matrices of the section and of the soil interfaces, respectively. Integration by parts of (23) and substitution of the equilibrium equation (5) lead to the following matrix equation:

$$\int_L \left\{ \begin{matrix} \delta \mathbf{D}_B(x) \\ \delta \mathbf{D}_s(x) \end{matrix} \right\}^T \begin{bmatrix} \mathbf{f}_B^0(x) & \mathbf{0} \\ \mathbf{0} & \mathbf{f}_s^0(x) \end{bmatrix} \left\{ \begin{matrix} \Delta \mathbf{D}_B(x) \\ \Delta \mathbf{D}_s(x) \end{matrix} \right\} dx = \delta \bar{\mathbf{Q}}^T \bar{\mathbf{U}} - \int_L \left\{ \begin{matrix} \delta \mathbf{D}_B(x) \\ \delta \mathbf{D}_s(x) \end{matrix} \right\}^T \left\{ \begin{matrix} \mathbf{d}_B^0(x) \\ \mathbf{d}_s^0(x) \end{matrix} \right\} dx \quad (24)$$

where  $\delta \bar{\mathbf{Q}}^T \bar{\mathbf{U}}$  is the boundary term and represents the external virtual work done by  $\delta \bar{\mathbf{Q}}$  (the virtual element nodal forces without rigid body modes) on  $\bar{\mathbf{U}}$  (the corresponding element nodal deformations, or displacements without rigid body modes). The element is formulated without rigid body modes in view of its implementation in a general-purpose finite element code, which requires inversion of the element flexibility matrix [14]. Eq. (24) is the fundamental equation of the force-based finite element formulation. To obtain the discrete form of (24), the section forces  $\mathbf{D}_B(x)$  and the soil-interface forces  $\mathbf{D}_s(x)$  are expressed in terms of the element nodal forces without rigid body modes  $\bar{\mathbf{Q}}$  and of the soil-interface forces  $\bar{\mathbf{Q}}_s$  at selected reference points along the interface, according to the following matrix relation:

$$\left\{ \begin{matrix} \mathbf{D}_B(x) \\ \mathbf{D}_s(x) \end{matrix} \right\} = \begin{bmatrix} \mathbf{N}_{BB}^{F-B}(x) & \mathbf{N}_{Bs}^{F-B}(x) \\ \mathbf{N}_{sB}^{F-B}(x) & \mathbf{N}_{ss}^{F-B}(x) \end{bmatrix} \left\{ \begin{matrix} \bar{\mathbf{Q}} \\ \bar{\mathbf{Q}}_s \end{matrix} \right\} \quad (25)$$

where the superscript F-B denotes the force-based formulation, and  $\mathbf{N}_{BB}^{F-B}(x)$ ,  $\mathbf{N}_{Bs}^{F-B}(x)$ ,  $\mathbf{N}_{sB}^{F-B}(x)$ ,  $\mathbf{N}_{ss}^{F-B}(x)$  are the force interpolation functions. Substitution of (25) into (24) and from the arbitrariness of  $\delta \bar{\mathbf{Q}}$  and  $\delta \bar{\mathbf{Q}}_s$ , the following matrix expression results:

$$\begin{bmatrix} \bar{\mathbf{F}}_{BB}^0 & \bar{\mathbf{F}}_{Bs}^0 \\ \bar{\mathbf{F}}_{Bs}^{0T} & \bar{\mathbf{F}}_{ss}^0 \end{bmatrix} \left\{ \begin{matrix} \Delta \bar{\mathbf{Q}} \\ \Delta \bar{\mathbf{Q}}_s \end{matrix} \right\} = \left\{ \begin{matrix} \bar{\mathbf{U}} \\ \mathbf{0} \end{matrix} \right\} - \left\{ \begin{matrix} \bar{\mathbf{r}}^0 \\ \bar{\mathbf{r}}_s^0 \end{matrix} \right\} \quad (26)$$

where  $\bar{\mathbf{F}}_{BB}^0$ ,  $\bar{\mathbf{F}}_{Bs}^0$ ,  $\bar{\mathbf{F}}_{ss}^0$  are the following flexibility terms:

$$\begin{aligned} \bar{\mathbf{F}}_{BB}^0 &= \int_L \left( \mathbf{N}_{BB}^{F-BT} \mathbf{f}_B^0 \mathbf{N}_{BB}^{F-B} + \mathbf{N}_{sB}^{F-BT} \mathbf{f}_s^0 \mathbf{N}_{sB}^{F-B} \right) dx \\ \bar{\mathbf{F}}_{Bs}^0 &= \int_L \left( \mathbf{N}_{BB}^{F-BT} \mathbf{f}_B^0 \mathbf{N}_{Bs}^{F-B} + \mathbf{N}_{sB}^{F-BT} \mathbf{f}_s^0 \mathbf{N}_{ss}^{F-B} \right) dx \\ \bar{\mathbf{F}}_{ss}^0 &= \int_L \left( \mathbf{N}_{Bs}^{F-BT} \mathbf{f}_B^0 \mathbf{N}_{Bs}^{F-B} + \mathbf{N}_{ss}^{F-BT} \mathbf{f}_s^0 \mathbf{N}_{ss}^{F-B} \right) dx \end{aligned} \quad (27)$$

$\bar{\mathbf{r}}^0$  and  $\bar{\mathbf{r}}_s^0$  represent the displacements at the element and soil degrees of freedom, respectively, compatible with the internal deformations  $\mathbf{d}_B^0$  and  $\mathbf{d}_s^0$

$$\bar{\mathbf{r}}^0 = \int_L \left( \mathbf{N}_{BB}^{F-B^T} \mathbf{d}_B^0 + \mathbf{N}_{sB}^{F-B^T} \mathbf{d}_s^0 \right) dx \quad (28)$$

$$\bar{\mathbf{r}}_s^0 = \int_L \left( \mathbf{N}_{Bs}^{F-B^T} \mathbf{d}_B^0 + \mathbf{N}_{ss}^{F-B^T} \mathbf{d}_s^0 \right) dx$$

Similarly to the element nodal force residuals in the stiffness equation (17),  $\bar{\mathbf{U}} - \bar{\mathbf{r}}^0$  and  $-\bar{\mathbf{r}}_s^0$  represent the element nodal and soil displacement residuals, respectively, in the flexibility equation (26). The zero term on the right-hand side of (26) implies that the relative soil-deformations at the selected reference points along the interfaces are equal to zero. This condition is similar to the known displacement conditions that are used to determine the redundant forces in statically indeterminate structures by the classical force method.

The redundant force unknowns  $\Delta \bar{\mathbf{Q}}_s$  are eliminated through static condensation in (26). The second equation in (26) yields  $\Delta \bar{\mathbf{Q}}_s = -(\bar{\mathbf{F}}_{ss}^0)^{-1} (\bar{\mathbf{F}}_{sB}^0 \Delta \bar{\mathbf{Q}} + \bar{\mathbf{r}}_s^0)$ , which substituted in the first equation yields

$$\bar{\mathbf{F}}^0 \Delta \bar{\mathbf{Q}} = \bar{\mathbf{U}} - \bar{\mathbf{U}}_B^0 - \bar{\mathbf{U}}_s^0 \quad (29)$$

where  $\bar{\mathbf{F}}$  is element flexibility matrix defined as

$$\bar{\mathbf{F}}^0 = \bar{\mathbf{F}}_{BB}^0 - \bar{\mathbf{F}}_{Bs}^0 (\bar{\mathbf{F}}_{ss}^0)^{-1} \bar{\mathbf{F}}_{sB}^0 \quad (30)$$

and  $\bar{\mathbf{U}}_B^0$ ,  $\bar{\mathbf{U}}_s^0$  are the contributions of the beam component and of the soil interfaces, respectively, to the element nodal displacements  $\bar{\mathbf{U}}^0$  without rigid body modes

$$\begin{aligned} \bar{\mathbf{U}}_B^0 &= \int_L \left( \mathbf{N}_{BB}^{F-B^T} - \bar{\mathbf{F}}_{Bs}^0 (\bar{\mathbf{F}}_{ss}^0)^{-1} \mathbf{N}_{Bs}^{F-B^T} \right) \mathbf{d}_B^0 dx \\ \bar{\mathbf{U}}_s^0 &= \int_L \left( \mathbf{N}_{sB}^{F-B^T} - \bar{\mathbf{F}}_{Bs}^0 (\bar{\mathbf{F}}_{ss}^0)^{-1} \mathbf{N}_{ss}^{F-B^T} \right) \mathbf{d}_s^0 dx \end{aligned} \quad (31)$$

The right-hand side vector  $\bar{\mathbf{U}} - \bar{\mathbf{U}}_B^0 - \bar{\mathbf{U}}_s^0$  of (29) represents the element nodal displacement residuals corresponding to the weak form of the compatibility conditions (7) and (9) vanishes when the compatible configuration is reached. In order to implement the force-based element in a general-purpose displacement-based finite element program, it is necessary to introduce a special state-determination procedure, which is discussed in detail in Limkatanyu and Spacone [12]. This procedure computes the element stiffness matrix and the resisting forces for the element without rigid body modes and then adds the rigid body modes back into the element. The resulting hybrid solution procedure, required to interface the force-based element formulation with the displacement-based structural solver, allowed the authors to rename the element formulation *force-hybrid*.

Fig. 6 shows the two-node force-based frame element with and without rigid body modes used in this study. Adding the rigid body modes to the element of Fig. 6(b) or filtering out the rigid body modes from the element of Fig. 6(a) is accomplished through matrix transformations

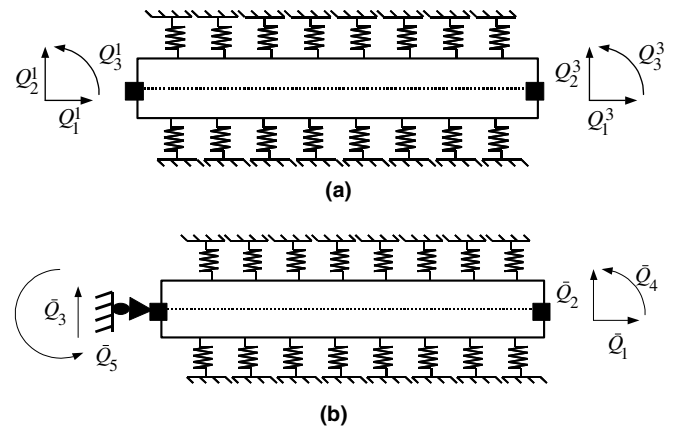


Fig. 6. Two-node force-based frame element with lateral deformable supports (a) with rigid body modes and (b) without rigid body modes.

based on equilibrium and compatibility between the two systems.

In structures that are internally statically determinate, such as the reinforced concrete beam with perfect bond of Spacone et al. [14], the internal force distributions can be determined exactly from equilibrium. In the beam model with lateral deformable supports of Fig. 6, which is internally statically indeterminate, the internal force distributions cannot be exactly determined from equilibrium only, except for some special, simple linear-elastic structures. The soil-interface forces serve as the redundant forces in this element. Assumptions on the soil force distributions are made. This procedure is identical to that followed by Salari et al. [15] for the steel–concrete composite beam with deformable shear connectors. In the proposed formulation of an element with lateral deformable supports, the soil-force distributions are assumed to be cubic functions. The bending moment distribution corresponding to the cubic soil-interface force distributions is a fifth-order polynomial.

### 3.3. Hellinger–Reissner mixed formulation

In the two-field mixed formulation, the section forces  $\mathbf{D}_B(x)$  are expressed in terms of the element nodal forces  $\mathbf{Q}_R$  through force interpolation functions, and the beam displacements  $\mathbf{u}(x)$  are expressed as functions of the element nodal displacements  $\mathbf{U}$  via displacement interpolation functions. The beam element nodal forces  $\mathbf{Q}_R$  and nodal displacements  $\mathbf{U}$  serve as the primary element variables. The equilibrium equation (5), and the beam compatibility equation (7) are satisfied in an integral (or weak) form. On the other hand, compatibility of the soil-interface field is satisfied in a strong form through the soil compatibility equation (9). The element formulation is based on the Hellinger–Reissner (H–R) mixed variational principle as discussed in Felippa [16] and Ayoub [17]. The mixed formulation is schematically represented in the Tonti’s diagram of Fig. 7. Based on the virtual displacement principle,

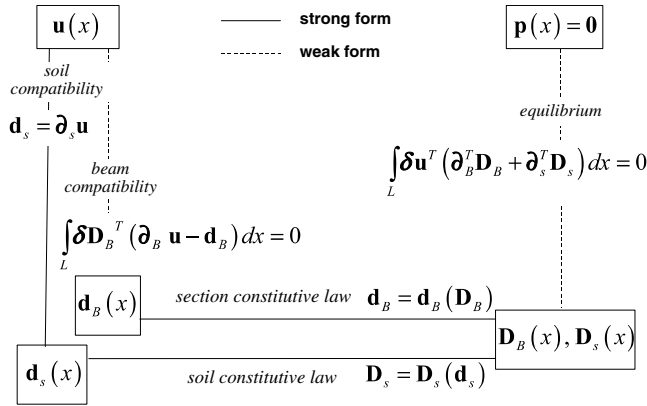


Fig. 7. Tonti's diagram for beam with lateral deformable supports: Hellinger–Reissner mixed formulation.

the weighted integral form of the equilibrium equation is expressed as

$$\int_L \delta \mathbf{u}^T(x) [\partial_B^T \mathbf{D}_B(x) + \partial_s^T \mathbf{D}_s(x)] dx = 0 \quad (32)$$

where  $\delta \mathbf{u}(x)$  is a compatible virtual displacement field. In order to move the differential operators  $\partial_B$  and  $\partial_s$  from the section forces  $\mathbf{D}_B(x)$  and soil-interface forces  $\mathbf{D}_s(x)$  to the virtual displacement field  $\delta \mathbf{u}(x)$ , integration by parts is applied to (32)

$$\int_L [(\partial_B \delta \mathbf{u}(x))^T \mathbf{D}_B(x) + (\partial_s \delta \mathbf{u}(x))^T \mathbf{D}_s(x)] dx = \delta \mathbf{U}^T \mathbf{P} \quad (33)$$

Upon application of the linear incremental form of the material constitutive law (10) and after imposing the soil-interface compatibility (9), (33) is written

$$\begin{aligned} & \int_L \delta \mathbf{u}^T(x) [\partial_B^T \Delta \mathbf{D}_B(x) + \partial_s^T \mathbf{k}_s^0(x) \partial_s \Delta \mathbf{u}(x)] dx \\ & = \delta \mathbf{U}^T \mathbf{P} - \int_L \delta \mathbf{u}^T(x) [\partial_B^T \mathbf{D}_B^0(x) + \partial_s^T \mathbf{D}_s^0(x)] dx \end{aligned} \quad (34)$$

Eq. (34) is the linear incremental form of the virtual displacement principle.

Based on the virtual force principle, the weighted integral form of the beam compatibility Eq. (7) can be written as

$$\int_L \delta \mathbf{D}_B^T(x) [\partial_B \mathbf{u}(x) - \mathbf{d}_B(x)] dx = 0 \quad (35)$$

where  $\delta \mathbf{D}_B(x)$  is a virtual equilibrated force field that serves as trial function. Upon substitution of (11) and after expressing the displacement field in its linearized form  $\mathbf{u}(x) = \mathbf{u}^0(x) + \Delta \mathbf{u}(x)$ , Eq. (35) is written

$$\begin{aligned} & \int_L \delta \mathbf{D}_B^T(x) [\partial_B \Delta \mathbf{u}(x) - \mathbf{f}_B^0(x) \Delta \mathbf{D}_B(x)] dx \\ & = \int_L \delta \mathbf{D}_B^T(x) [\mathbf{d}_B^0(x) - \partial_B \mathbf{u}^0(x)] dx \end{aligned} \quad (36)$$

Eqs. (34) and (36) form the fundamental equations of the H–R mixed finite element formulation for the frame

element with lateral deformable supports. They are combined into the following form:

$$\begin{aligned} & \int_L \left\{ \begin{matrix} \delta \mathbf{u}(x) \\ \delta \mathbf{D}_B(x) \end{matrix} \right\}^T \left[ \begin{matrix} \partial_s^T \mathbf{k}_s^0(x) \partial_s & \partial_B^T \\ \partial_B & -\mathbf{f}_B^0(x) \end{matrix} \right] \left\{ \begin{matrix} \Delta \mathbf{u}(x) \\ \Delta \mathbf{D}_B(x) \end{matrix} \right\} dx \\ & = \delta \mathbf{U}^T \mathbf{P} - \int_L \left\{ \begin{matrix} \delta \mathbf{u}(x) \\ \delta \mathbf{D}_B(x) \end{matrix} \right\}^T \left\{ \begin{matrix} \partial_B^T \mathbf{D}_B^0(x) + \partial_s^T \mathbf{D}_s^0(x) \\ \partial_B \mathbf{u}^0(x) - \mathbf{d}_B^0(x) \end{matrix} \right\} dx \end{aligned} \quad (37)$$

To obtain the discrete form of (37), the beam force and displacement fields are expressed in terms of the nodal force degrees of freedom  $\mathbf{Q}_R$  (to be defined later in the paper) and the nodal displacements  $\mathbf{U}$  through the force and displacement interpolation functions, respectively

$$\begin{aligned} \mathbf{u}(x) &= \mathbf{N}_u^{\text{H-R}}(x) \mathbf{U} \\ \mathbf{D}_B(x) &= \mathbf{N}_F^{\text{H-R}}(x) \mathbf{Q}_R \end{aligned} \quad (38)$$

where superscript H–R denotes the H–R mixed formulation.  $\mathbf{N}_u^{\text{H-R}}(x)$  contains the displacement interpolation functions for the beam displacements and  $\mathbf{N}_F^{\text{H-R}}(x)$  contains the force interpolation functions for the beam forces. Upon substitution of (38) into (37) and from the arbitrariness of  $\delta \mathbf{Q}_R$  and  $\delta \mathbf{U}$  the following mixed equation results:

$$\left[ \begin{matrix} \mathbf{K}_s^0 & \mathbf{T}^T \\ \mathbf{T}^T & -\bar{\mathbf{F}}_B^0 \end{matrix} \right] \left\{ \begin{matrix} \Delta \mathbf{U} \\ \Delta \mathbf{Q}_R \end{matrix} \right\} = \left\{ \begin{matrix} \mathbf{P} - \mathbf{T}^T \mathbf{Q}_R^0 - \mathbf{Q}_s^0 \\ \bar{\mathbf{U}}_{Rr}^0 \end{matrix} \right\} \quad (39)$$

where  $\mathbf{K}_s^0$  is the contribution of the soil interfaces to the element stiffness matrix, defined as

$$\mathbf{K}_s^0 = \int_L \mathbf{B}_s^{\text{H-R}^T}(x) \mathbf{k}_s^0(x) \mathbf{B}_s^{\text{H-R}}(x) dx \quad (40)$$

with  $\mathbf{B}_B^{\text{H-R}}(x) = \partial_B \mathbf{N}_u^{\text{H-R}}(x)$ ,  $\mathbf{B}_s^{\text{H-R}}(x) = \partial_s \mathbf{N}_u^{\text{H-R}}(x)$ .  $\bar{\mathbf{F}}_B^0$  is the beam flexibility matrix, defined as

$$\bar{\mathbf{F}}_B^0 = \int_L \mathbf{N}_F^{\text{H-R}^T}(x) \mathbf{f}_B^0(x) \mathbf{N}_F^{\text{H-R}}(x) dx \quad (41)$$

Matrix  $\mathbf{T}$  serves as the transformation matrix between the force degrees of freedom and the displacement degrees of freedom, and is defined as

$$\mathbf{T} = \int_L \mathbf{N}_F^{\text{H-R}^T}(x) \mathbf{B}_B^{\text{H-R}}(x) dx \quad (42)$$

$\bar{\mathbf{U}}_{Rr}^0$  contains the beam nodal displacement residuals and is defined as

$$\bar{\mathbf{U}}_{Rr}^0 = \int_L \mathbf{N}_F^{\text{H-R}^T}(x) \mathbf{d}_B^0(x) - \mathbf{T} \mathbf{U}^0 \quad (43)$$

$\mathbf{Q}_s^0$  is the contribution of the soil interfaces to the element forces

$$\mathbf{Q}_s^0 = \int_L \mathbf{B}_s^{\text{H-R}^T}(x) \mathbf{D}_s^0(x) dx \quad (44)$$

The right-hand side of (39) contains the force and displacement residuals, which correspond to the weighted integral forms of equilibrium and of beam compatibility, respectively.

In view of the element implementation into a general-purpose finite element program, the force degrees of freedoms in (39) are eliminated using static condensation. Consequently, the force continuity between adjacent elements is locally relaxed. From the second equation in (39) the beam element nodal forces are computed as  $\Delta \mathbf{Q}_R = (\bar{\mathbf{F}}_B^0)^{-1}(\mathbf{T}\Delta \mathbf{U} - \bar{\mathbf{U}}_{Rr}^0)$  and they are substituted into the first equation in (39) to obtain

$$(\mathbf{T}^T (\bar{\mathbf{F}}_B^0)^{-1} \mathbf{T} + \mathbf{K}_s^0) \Delta \mathbf{U} = \mathbf{P} - \mathbf{T}^T \mathbf{Q}_R^0 - \mathbf{Q}_s^0 + \mathbf{T}^T (\bar{\mathbf{F}}_B^0)^{-1} \bar{\mathbf{U}}_{Rr}^0 \quad (45)$$

where the term  $\mathbf{T}^T \mathbf{Q}_R^0 + \mathbf{Q}_s^0 - \mathbf{T}^T (\bar{\mathbf{F}}_B^0)^{-1} \bar{\mathbf{U}}_{Rr}^0$  represents the element forces. In (45),  $\mathbf{Q}_s^0$  are the forces directly dual to the nodal displacements  $\mathbf{U}$ , while  $\mathbf{Q}_R^0$  and  $(\bar{\mathbf{F}}_B^0)^{-1} \bar{\mathbf{U}}_{Rr}^0$  represent the nodal forces at the force degrees of freedom. These latter are pre-multiplied by the transformation matrix  $\mathbf{T}$  to become dual to the nodal displacements  $\mathbf{U}$ .

In order to ensure numerical stability of the solution, the element degrees of freedom and the element displacement and force interpolation functions cannot be arbitrarily selected for mixed elements, as discussed in Zienkiewicz and Taylor [18]. Ayoub [17] discusses the stability issue for two-field mixed beam elements. The stability condition requires that

$$n_R \geq n_U \quad (46)$$

where  $n_R$  is the number of force degrees of freedom and  $n_U$  is the number of displacement degrees of freedom of the element without rigid body modes. The above condition is necessary but not sufficient to ensure element convergence.

The degree of the displacement interpolation functions was selected in this study after considering the variational indices in (35). Because the first derivative of the axial displacement and the second derivative of the transverse displacement appear in (35),  $C^0$  and  $C^1$  continuous functions are used for the axial and transverse displacements, respectively. As a result, a cubic Hermitian polynomial is used for the beam transverse displacement and quadratic polynomials are used for the beam axial displacement. Because the cubic transverse displacement implies a linear curvature variation and the quadratic axial displacement implies a linear axial strain variation, linear bending moment and axial force variations were selected for the force interpolation functions.

The displacement degrees of freedom that derive from the above considerations are shown in Fig. 8(a). The displacement degrees of freedom use a three-node beam element. Each end node has three degrees of freedoms. The middle node has the axial displacement degree of freedom only. As a result, the axial displacement distribution in the beam is quadratic; the transverse displacement distribution in the beam is cubic and the soil-deformation distribution is cubic.

The two-node beam is used to define the element force degrees of freedoms without rigid body modes (Fig. 8(b)). Each node has two degrees of freedoms, one for the axial

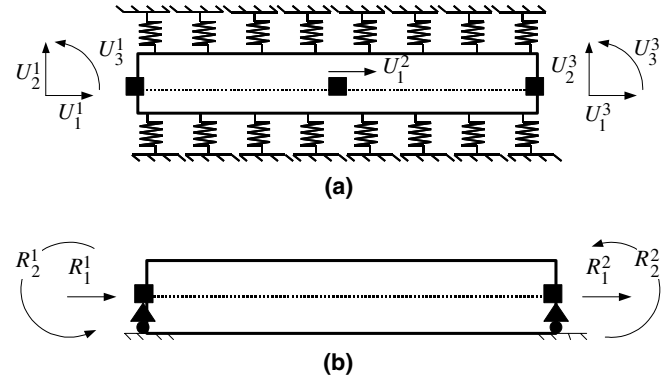


Fig. 8. Mixed element with lateral deformable supports (a) displacement degrees of freedom and (b) force degrees of freedom.

force and one for the bending moment in the beam. The nodal force components  $R$  in Fig. 8(b) are grouped in the beam nodal force vector  $\mathbf{Q}_R$ . Consequently, the beam axial force and the beam bending moment are both linear.

#### 4. Numerical validation

The simply supported beam on lateral deformable foundation of Fig. 9 is used to investigate the performance and the characteristics of the aforementioned nonlinear frame elements. Due to symmetry, only half of the beam is used for the analyses. The beam geometric characteristics are shown in Fig. 9. The beam section is discretized into 20 fibers. Each fiber has a nonlinear elastic-strain hardening uniaxial constitutive law, with initial modulus of elasticity 210 GPa and yield strength 460 MPa. The strain-hardening ratio is 0.01. The  $p$ - $y$  curve of the soil foundation is assumed to be elasto-plastic. The yield displacement is 40 mm., the corresponding yield pressure is 40 MPa, and the strain-hardening ratio is 0.05. The nonlinear analyses are performed under displacement control.

Fig. 10 shows the results of an investigation on the number of elements required to reach the converged solution for the three formulations presented in this paper. The three plots illustrate the midspan  $P$ - $\delta$  (force-displacement) responses. The so-called “benchmark” response is obtained with a mesh consisting of 32 displacement-based elements. The changes in the response slopes are due to yielding of the beam first and yielding of the foundation springs next. Fig. 10(a) presents the responses obtained with different meshes of displacement-based elements. It is seen that for meshes of more than 16 elements, the responses do not further change, showing that the converged solution has been reached. Fig. 10(b) shows the convergence characteristics of the force-based (force-hybrid) element. The force-based element is much more accurate than the displacement-based element, and only two elements are required to reach the converged solution, with one element providing already a satisfactory response. Likewise, Fig. 10(c) indicates that the H-R mixed element is rather accurate, as shown by

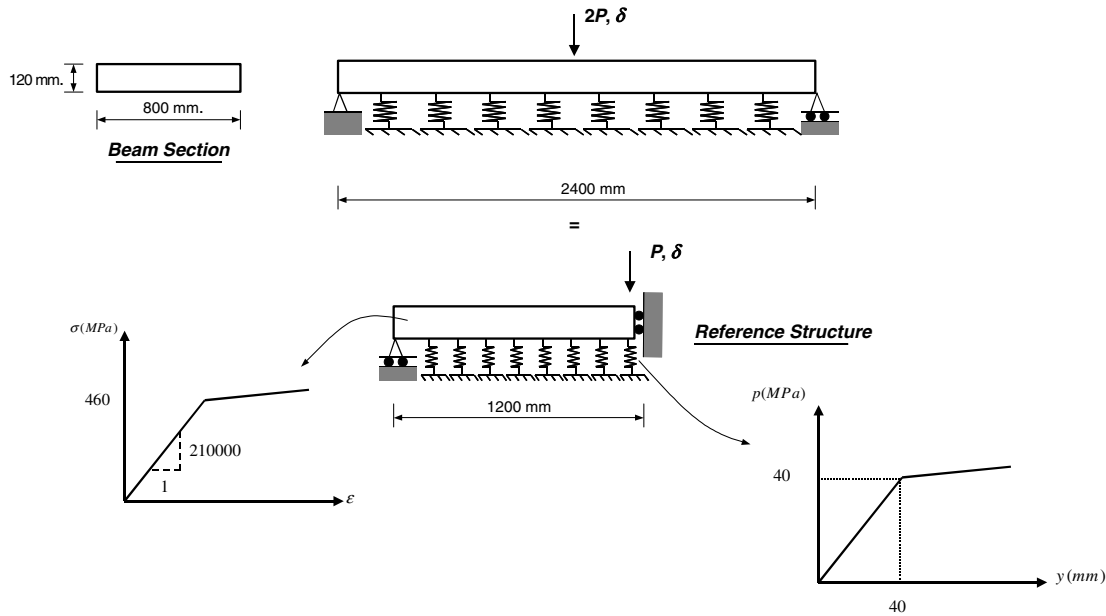


Fig. 9. Simply supported beam on lateral deformable foundation.

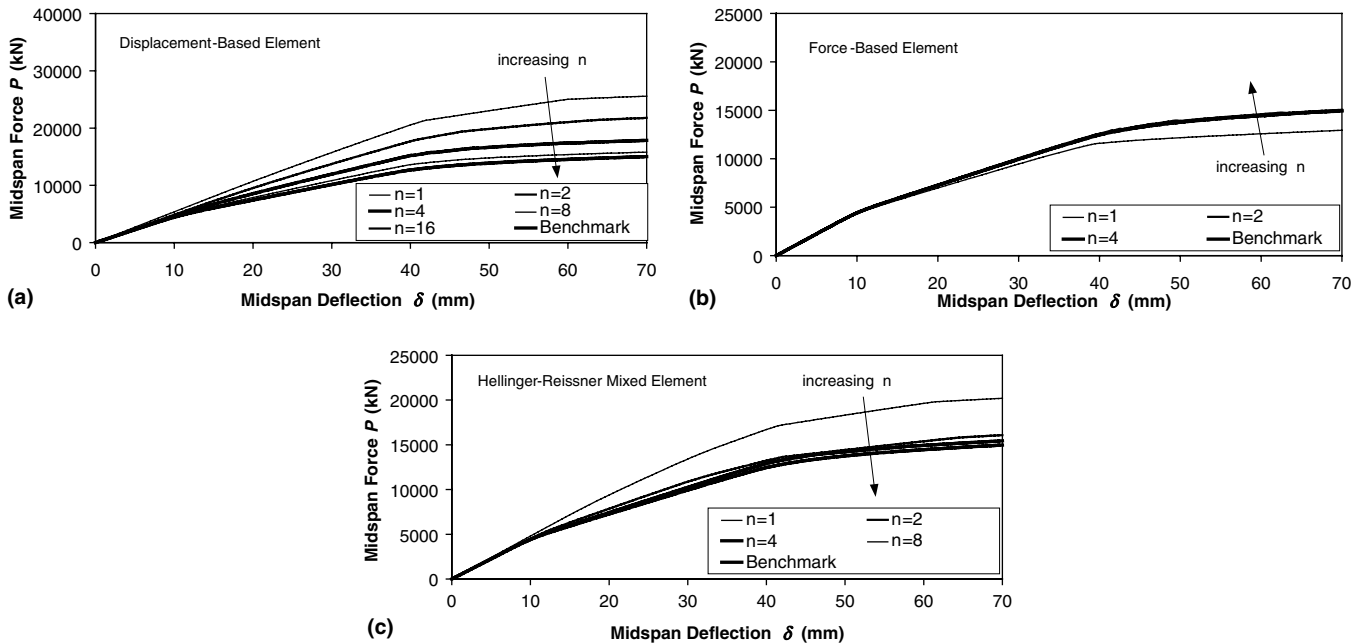


Fig. 10. Convergence study of the three frame elements with lateral deformable supports.

the increase in accuracy after the first decrease in response stiffness ( $\delta = 10$  mm) for meshes comprised of two, four, and eight elements.

It is interesting to point out that for the displacement-based element, in which the displacements serve as the primary variables, a more refined mesh leads to a more flexible response (convergence from above), while for the force-based element, in which the forces serve as primary variables, a more refined mesh results in a stiffer response (convergence from below). For the H–R mixed element

in which both displacements and forces serve as the primary variables, the response converges from above, indicating that the displacement interpolation functions  $N_u^{H-R}$  play a role which is more essential than that of the force interpolation functions  $N_F^{H-R}$  in controlling the element response. The assumed force interpolation functions, however, enhance the element accuracy. This happens because, in general, the force fields along the beam are smoother than the deformation fields, which may show large jumps in the inelastic regions, particularly where plastic

hinges tend to form. For the results of Fig. 10, the central processing unit (CPU) times on a Pentium IV 1.3 GHz personal computer and the errors of the three aforementioned element formulations with different element numbers are presented in Table 1. The errors were measured based on the following expression:

$$e = \frac{\sum_{k=1}^{N_{\text{step}}} \left| \frac{P_{y_k} - P_{y_k}^{\text{exact}}}{P_{y_k}^{\text{exact}}} \right|}{N_{\text{step}}} \times 100 \quad (47)$$

where  $e$  represents the percentage error,  $N_{\text{step}}$  is the number of applied displacement steps used in the analysis (this number is the same for all analyses of Fig. 9).  $P_{y_k}$  are the midspan forces at step  $k$  and  $P_{y_k}^{\text{exact}}$  represent the “benchmark” forces at the same step. The results of Table 1 further highlight the better accuracy in terms of computational cost of the

force-based and H–R mixed elements. The CPU time of a single force-based element is almost twice that of a single displacement-based element, while the CPU time of the mixed element is comparable to that of the displacement-based element. A further study compares the CPU time necessary to reach convergence. Convergence is defined when the above-defined error  $e$  is smaller than 1.5%. The use of force-based elements leads to the lowest CPU time (because only two elements are required), while the displacement-based elements lead to the slowest solution (because 18 elements are needed to reach convergence). Six mixed elements are needed to reach convergence, with a convergence time slightly higher than that of the force-based element.

Fig. 11 shows the distributions of the beam curvature, beam moment, soil-deformation (vertical deflection) and soil-force at the integration points along the beam

Table 1  
CPU time (on a Pentium IV 1.3 GHz PC) and number of elements needed for convergence for the beam of Fig. 9

| Number of elements | Displacement-based |             | Force-based  |             | Hellinger–Reissner |             |
|--------------------|--------------------|-------------|--------------|-------------|--------------------|-------------|
|                    | CPU time (s)       | (Error) (%) | CPU time (s) | (Error) (%) | CPU time           | (Error) (%) |
| 1                  | 2.52               | (56.46)     | 4.48         | (2.99)      | 3.48               | (28.4)      |
| 2                  | 4.34               | (35.74)     | 9.19         | (0.33)      | 6.92               | (5.38)      |
| 4                  | 8.16               | (17.19)     | Converged    |             | 9.38               | (1.78)      |
| 6                  | –                  |             | –            |             | 11.08              | (0.83)      |
| 8                  | 15.62              | (6.02)      |              |             | Converged          |             |
| 16                 | 31.02              | (1.29)      |              |             |                    |             |
|                    | Converged          |             |              |             |                    |             |

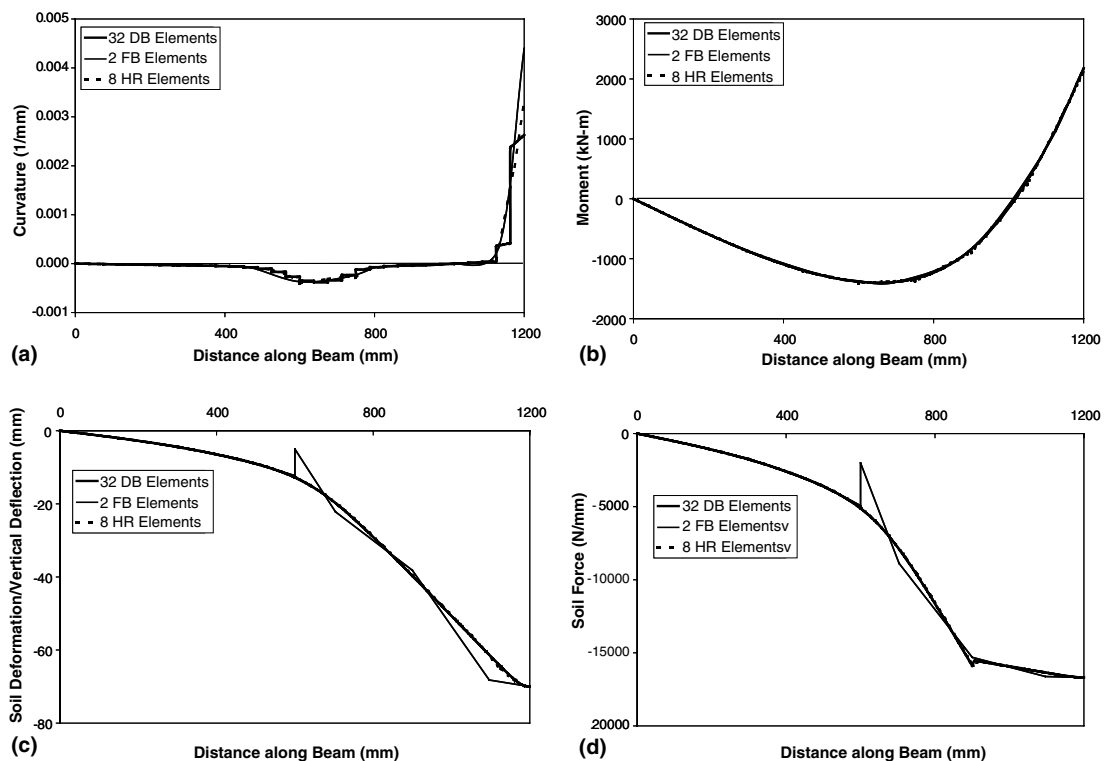


Fig. 11. Internal field distributions at integration points for midspan displacement  $\delta = 70$  mm.

associated with a midspan deflection  $\delta = 70$  mm. The response with 32 displacement-based elements serves as reference solution. In order to have a sufficient number of points of internal force and deformation distributions, the number of elements is increased from six to eight for the H–R mixed element. Clearly, the results of Fig. 11 indicate that the force-based and H–R mixed elements are capable of representing not only the global (Fig. 10) but also the local response.

In order to observe the different characteristics of the three element formulations, Fig. 12 shows a close-up look of the internal field distributions of Fig. 11. The plots of Fig. 12 are limited to the 400–800 mm distance along the beam and the response scales are also modified. For the displacement-based element, there are discontinuities in the curvature and moment distributions between adjacent elements, because neither compatibility nor equilibrium is enforced between the two end sections of two adjacent elements. It is worth pointing out that the Gauss–Lobatto integration scheme is used in the element implementations, thus each one of the two beam elements sharing a node has a monitored section located at the nodal coordinates. The jump in the moment distribution between adjacent elements is rather small in Fig. 12(b) and is not clearly visible. There is, however, continuity in the soil-deformation (vertical deflection) and soil-force distributions between adjacent elements, because the soil compatibility equation is imposed in the point-wise sense. Similar discontinuities in curvature and moment distributions are also found for the H–R mixed element. This, however, is the result of the condensation of the nodal force degrees of freedom,

mentioned earlier in the element formulation. There is continuity in the soil-deformation (vertical deflection) and soil-force distributions between adjacent elements due to the satisfaction of the soil compatibility condition in the strong sense. For the force-based element, the curvature and moment distributions are continuous between adjacent elements. This is due to the fact that since the nodal forces are in equilibrium, and because the internal force distributions are in equilibrium with the nodal forces through the force interpolation functions, the internal force distributions are continuous. Because the section deformations in the force-based element are obtained from the section forces through the section constitutive law, the section deformations (curvature in this case) are also continuous. On the other hand, there exist discontinuities in soil-deformation and soil-force distributions between adjacent elements, because the reference soil-forces are condensed out as outlined in the element formulation.

Of great interest is also the capability of the proposed frame elements to trace the softening response due to softening of the soil foundation. Consequently, the hardening soil foundation of the beam in Fig. 9 is replaced by a softening soil foundation. The softening branch of the  $p$ – $y$  curve of the soil foundation is assumed to be linear. The yield displacement is 40 mm, associated with the 40-MPa yield pressure and the ultimate displacement is 120 mm, associated with the zero pressure. The load–displacement diagram obtained with the three models is shown in Fig. 13. For the displacement-based model, the beam is discretized into 32 elements. For the force-based model, there are four elements in the beam. Finally, eight elements are

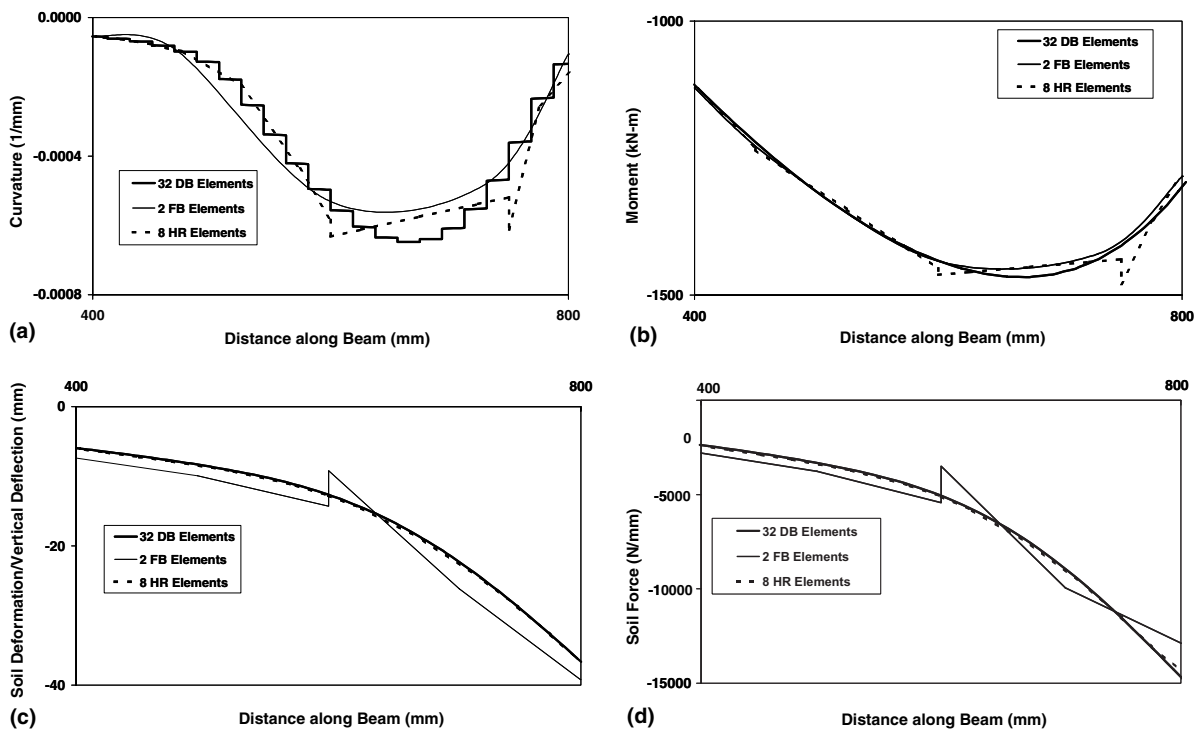


Fig. 12. A close-up look of internal field distributions in Fig. 11.

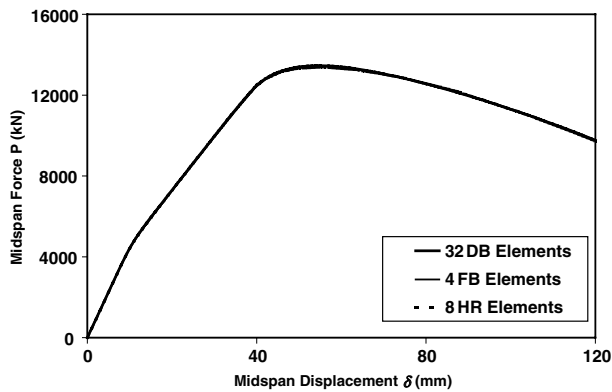


Fig. 13. Load–displacement response of simply supported beam in Fig. 9 on lateral softening supports.

used to discretize the beam in the H–R model. The three proposed models succeeded in detecting the softening behavior of the beam with the softening soil foundation. The force-based model shows an advantage in term of the computational expense. However, it is important to note that the midspan displacement of the force-based model cannot exceed 120 mm. (associated with the zero foundation stiffness) due to the fact that the soil-section stiffness matrix needs to be inverted during the element state determination. On the other hand, the midspan displacement can go beyond 120 mm. in both displacement-based and the H–R mixed models, because the lateral-soil behavior is derived from the displacement shape functions, and thus the soil-section stiffness does not need to be inverted.

## 5. Conclusions and future work

The paper presents a family of three frame elements capable of modeling a nonlinear beam element on nonlinear deformable supports. The formulation starts from the derivation of the governing differential equations (strong form) and then, three different finite element formulations (weak forms) are derived. The three finite elements are based on the displacement-based, the force-based (hybrid), and the Hellinger–Reissner mixed formulations. The displacement-based element is derived from the virtual displacement principle and uses displacement interpolation functions to express the beam and lateral-soil displacement fields in term of nodal displacement degrees of freedom. The force-based (hybrid) element is derived from the virtual force principle and employs force interpolation functions to express the internal force fields in terms of force degrees of freedom. In this element, the element soil-forces at selected reference points serve as internal redundant forces. The Hellinger–Reissner mixed element is derived from the two-field mixed variational principle involving both the virtual displacement and virtual force principles. Force interpolation functions are used to express the beam internal force fields in terms of the beam force degrees of

freedom and displacement interpolation functions are used to express the soil-deformation fields in terms of the element displacement degrees of freedom.

A numerical example is used to compare the performance and characteristics of each finite element formulation. The results of the numerical example show the far superior accuracy of the force-based and Hellinger–Reissner mixed elements. Although a single displacement-based element is much faster than the other two elements, a much more refined mesh of displacement-based elements is required to reach the converged solution, resulting in high computational times. In the displacement-based element, the foundation force and deformation distributions are continuous between adjacent elements due to the strong imposition of the foundation compatibility. The moment and curvature distributions, however, are discontinuous over adjacent elements due to the weak enforcement of equilibrium. In the force-based element, the foundation force and deformation distributions are discontinuous between adjacent elements due to the static condensation of the element soil forces. The moment and curvature distributions, however, are continuous over adjacent elements due to the strong enforcement of equilibrium. In the Hellinger–Reissner mixed element, the foundation force and deformation distributions over adjacent elements are continuous due to the strong satisfaction of the soil compatibility. The moment and curvature distributions are discontinuous over adjacent elements due to the condensation of the element force degrees of freedoms.

The case of the beam on softening soil foundation is used to show the models' ability to represent the softening behavior of the beam/foundation system. Though all proposed models succeed in representing the softening response of the softening beam/foundation system, the force-based and mixed models are far more accurate. However, the force-based model encounters numerical problems when the lateral soil stiffness approaches singularity. No such problems are encountered in either displacement-based or Hellinger–Reissner models. It appears therefore that the H–R mixed model represents the best compromise between accuracy and numerical stability for the case of a hardening beam on a softening soil foundation.

The development of the proposed frame elements with lateral deformable supports is a step forward in establishing a computational framework that permits the full nonlinear static and dynamic analysis of frame structures including the soil–pile interaction effects. The next steps in this direction are the implementation of realistic  $p$ – $y$  curves capable of reproducing the most relevant experimentally observed phenomena and the development of a superstructure–pile cap–piles system for modeling the response of bridges subjected to ground motions.

## Acknowledgements

Special thanks go to Dr. Mohammed R. Salari for his assistance with formulations of beams with lateral

deformable supports and to Professor Carlos A. Felippa of the Aerospace Engineering Department of the University of Colorado, Boulder for his continuous support on theoretical issues. This study was partially supported by the Thai Ministry of University Affairs (MUA), by the Thailand Research Fund (TRF) under Grant MRG4680109, by the National Science Foundation under Grant No. CMS-0010112 and by the Italian Ministry of Education, University and Research (MIUR) under a Cofin Grant. This support is gratefully acknowledged. Any opinions expressed in this paper are those of the authors and do not reflect the views of the sponsoring agencies.

The first author would like to dedicate this work to his late father for the life-long love and unconditional support. He especially owes his father for teaching him to embark on life with dignity and to work hard to earn only the best outcome.

## References

- [1] Mindlin RD. Force at a point in the interior of a semi-infinite solid. *Physics* 1936;7:195–202.
- [2] Spillers JB, Stoll RD. Lateral response of piles. *J Soil Mech Found Div, ASCE* 1964;90(6):1–9.
- [3] Poulos HG. Behavior of laterally loaded piles: Part I—single piles. *J Soil Mech Found Div, ASCE* 1971;97(5):711–31.
- [4] Desai CS, Appel GC. 3-D analysis of laterally loaded structures. 2nd international conference on numerical methods in geomechanics. Blacksburg: ASCE; 1976.
- [5] Kuhlemeyer RL. Static and dynamic laterally loaded floating piles. *J Geotech Eng Div, ASCE* 1979;105(2):289–304.
- [6] Winnicki LA, Zienkiewicz OC. Plastic (or visco-plastic) behavior of axisymmetric bodies subjected to non-symmetric loading—semi-analytical finite element solution. *Int J Numer Meth Eng* 1979;14:1399–412.
- [7] Yang Z, Jeremic B. Numerical analysis of pile behavior under lateral loads in layered elastic–plastic soils. *Int J Numer Anal Meth Geomech* 2002;26(14):1385–406.
- [8] Budek AM, Priestley MJN, Benzoni G. Inelastic seismic response of bridge drilled-shaft RC pile/columns. *J Struct Eng, ASCE* 2000;126(4):510–7.
- [9] Hoit MI, McVay M, Hays C, Andrade PW. Nonlinear pile foundation analysis using Florida-Pier. *J Bridge Eng, ASCE* 1996; 1(4):135–42.
- [10] Mitchell JS. A nonlinear analysis of biaxially loaded beam-columns using a discrete element model, PhD dissertation, Department of Civil Engineering, University of Texas, Austin, 1973.
- [11] Limkatanyu S, Spacone E. R/C Frame element with bond interfaces. Part I: displacement-based, force-based and mixed formulations. *J Struct Eng, ASCE* 2002;123(3):346–55.
- [12] Limkatanyu S, Spacone E. R/C Frame element with bond interfaces. part II: stat determination and numerical validations. *J Struct Eng, ASCE* 2002;123(3):356–64.
- [13] Taylor, RL. FEAP: a finite element analysis program. User manual: version 7.3, Department of Civil and Environmental Engineering, University of California, Berkeley, 2000.
- [14] Spacone E, Filippou FC, Taucer FF. Fibre beam-column model for nonlinear analysis of R/C frames: Part I—formulation. *Earthquake Eng Struct Dynam* 1996;25:711–25.
- [15] Salari MR, Spacone E, Shing PB, Frangopol DM. Nonlinear analysis of composite beams with deformable shear connectors. *J Struct Eng, ASCE* 1998;124(10):1148–58.
- [16] Felippa CA. ASEN 5367 course notes: advanced finite element methods. Department of Aerospace Engineering, University of Colorado, Boulder, 2000.
- [17] Ayoub A. A two-field mixed variational principle for partially connected composite beams. *Finite Elem Anal Des* 2001;37:929–59.
- [18] Zienkiewicz OC, Taylor RL. The finite element method vol. I: the basis. 5th ed. Oxford: Butterworth–Heinemann; 2000.